Faculteit Technische Natuurwetenschappen

TU Delft

Coherent Structures in a Rod-Bundle Geometry

Faculteit Technische Natuurwetenschappen

TU Delft

Naam:	Felix Carlier		
Studentnummer:	1526154		
Opleiding:	Technische Natuurkunde		
Begeleider:	L. Portela	**Sectie:**	TP/NERA
2de beoordelaar:	M. Rohde		
Startdatum:	10 -09-2012	**Einddatum:**	26-08-2013
Is vertrouwelijkheid van toepassing?			

Delft University of Technology

Bachelor Project

Coherent Structures in a Rod-Bundle Geometry

Author:
Félix Carlier

Supervisors:
Dr. L. Portela
Dr. M. Rohde

August 20, 2013

Chapter 1

Abstract

Improvement of safety in nuclear reactors is of paramount importance to secure the future development of nuclear energy. The flow of water through a reactor is critical for heat and power dissipation. However, research on cross-flow mixing in a rod-bundle geometry at transitional and laminar flow is limited. The aim of this study is to acquire more insight on the structural cross-flow mixing of water in a rod-bundle geometry.

This study was performed using the same experimental set-up as Bulk (2012). The main goal was to identify coherent structures in single-phase flow in a Rod-Bundle Geometry. The study has been conducted at Reynolds numbers ranging from 500 Re to 6000 Re to obtain diversified results in the turbulent and laminar flow regions. Thorough analysis was concentrated on a flow at Reynolds 3000.

The experimental results were inconclusive for laminar flow. Results in this regime have been unpredictable, but have provided insights into the limitations of the measurement set-up. Encouraging results have been found for flows in the turbulent region. Spectral density analysis has provided a measure for the structure lengths. Correlation of the wire-mesh data has given an indication of the structure width at Reynolds 3000.

This study has provided essential insight in the experimental set-up and analysis methods for future flow studies. Furthermore, an estimate of structure length and width has been found.

Contents

Chapter 2

Introduction

Energy shortages are expected to arise in the coming decades. This forecast leads to a need in research in the the field of new alternative nuclear reactors. One of these areas of research is in the field of thermal-hydraulics in a reactor cores. The flow of coolant in reactor cores play a major role in the transport of energy and stabilization of reactors. This research aims to study the flow of water inside pressurised water reactors (PWR).
The importance of this study can be traced back to the removal of heat in a reactor. To maintain the reactor at a safe and stable temperature and, at the same time, operate at maximum efficiency, the stability and control of the heat removal is of great importance. The secondary flow and cross-channel flow of water in this geometry promotes the heat removal in the radial direction. This research will concentrate on the analysis of cross-flow in a rod-bundle geometry. Although the theoretical and computational approach are very interesting, this study was solely performed on an experimental basis.

The set-up as used in this experiment provides deeper insight in the dynamic flows in a rod-bundle geometry. This research is a continuation of the study by Bulk (2012) and uses the same geometry as Mamhood (2011) and van Campen (2009).

2.1 Previous work

Previous work on flow in a rod-bundle geometry was done by Ikeno, where he conducted research on secondary flow and cross-flow at several rod-diameter to pitch ratios. Mamhood conducted

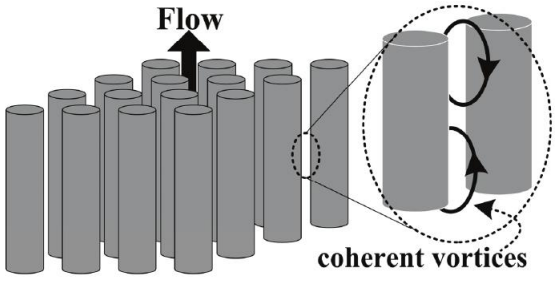

Figure 2.1: The Rod-Bundle geometry, and the location of the coherent structures is indicated.

research on several geometries, including the rod-bundle geometry, with the use of LDA and PIV. He further modelled the cross-flow through different geometries. Lastly Bulk investigated the cross-flow in a rod-bundle geometry using two wire-meshes. The study presented here, is continuation of the research by Bulk. This study differentiates itself from the previous work of Mahmood (2011) through the use of two wire-meshes. The use of two different wire meshes enables to acquire localized tracer velocities by cross-correlation of the time signals of both wire-meshes and will lead to more accurate results. A similar setup has been used by Ylönen et al. (2011) and first results were obtained of the dissipation through the channels.

Chapter 3

Theory

Since the industrialization the research in pipe-flow has taken great leaps. While regular pipe-flow characteristics are well documented, research on fluid flow through different geometries is still of great importance to modern day fluid dynamics. This chapter introduces important theoretical principles of flow to clarify the background of this study.

3.1 Pipe Flow

The characteristics of flow can be described mathematically by the Navier-Stokes equations. These equations specify the relation of stresses in the fluid with the pressure and viscous effects.

$$\frac{\partial U}{\partial t} + U \cdot \nabla U = -\frac{1}{\rho}\nabla P + \nu \nabla^2 U + f \tag{3.1}$$

with ρ the fluid density, P the pressure, ν the kinematic viscosity and f the body force.

Fluid flow can be categorized into two different sorts of flow regimes. The first regime is the laminar flow regime. At this regime the fluid flows in smooth parallel layers. No lateral motion of particles occur, because the shear stresses along the flow are not large enough. The second flow regime is called turbulent, figure 3.1b. This type of flow can be seen as more chaotic. The smooth flow lines of laminar flow are disturbed by shear stresses and form eddies. This form of flow incites mixing in all directions of the flow.

At certain flow rates a third type of flow regime can be distinguished. This form is called transitional flow, and describes the flow of fluid at the transition between laminar and turbulent flow. The flow is not as smooth and regular as laminar flow, showing signs of instabilities. However, turbulent flow is not yet fully developed at this stage.

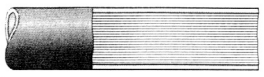

(a) Parallel flow lines at laminar flow regimes.

(b) Unstable flow lines at turbulent flow regimes.

Figure 3.1: Laminar and turbulent flow regimes in pipeflow.

To fully understand the properties of flow, the Reynolds number is introduced. The Reynolds number is a dimensionless number that defines the ratio between inertial forces and viscous forces. It is the most preferred property to describe the flow rate.

$$Re = \frac{UD}{\nu} \tag{3.2}$$

Lower Reynolds numbers indicate laminar flow, while higher Reynolds numbers defines turbulent flow. The transition, however, is dependent on the medium and geometry.

At turbulent flow regimes the formed unstable eddies break off into smaller sized eddies, thereby transferring their energy. These eddies in turn transfer their energy to even smaller eddies until the energy is dissipated through viscous diffusion. This process forms a wide range of different eddy sizes present in turbulent flow. The largest sizes are of the same order of magnitude as the hydraulic diameter, defined by equation 3.1, while the smallest sizes present in the flow are defined by the Kolmogorov equations, Kundu and Cohen (2000).

$$D_h = \frac{4A}{Q} \tag{3.3}$$

$$\eta \equiv \left(\frac{\nu^3}{\epsilon}\right)^{\frac{1}{4}}, \qquad u_\eta \equiv (\epsilon\nu)^{\frac{1}{4}}, \qquad \tau_\eta \equiv \left(\frac{\nu}{\epsilon}\right)^{\frac{1}{2}}. \tag{3.4}$$

The typical Kolmogorov scales ar in the order of μm

3.2 Rod-Bundle Flow

The importance of the research in this geometry is to help to quantify the radial heat dissipation. Three flow mechanisms are key to the heat dissipation, and will be shorty introduced.

First the regular heat-dissipation occurs. The second mechanism describes the flow perpendicular to the bulk flow, and is called secondary flow. Due to the nature of the geometry the flow can be considered as inhomogeneous thereby causing lateral stresses to occur between different areas. These stresses incite a flow perpendicular to the bulk flow that accelerates the cross sectional dissipation of a scalar. The last mechanism, known as cross-flow is the essence of this research and is described by coherent structures between gaps and sub-channels.

3.2.1 Structures

This mechanism is considered to be much more dominant then the secondary flow, and is therefore of great importance to research. Rowe et al. (1974) showed that macroscopic mixing processes played a mayor role in the mixing of fluids through a rod-bundle geometry. Ikeno and Kajishima (2010), Mahmood (2011), and Bulk (2012) researched the presence of cross-flow structures and had promising results. These structures occur due to instabilities between the flow-lines in the gaps and those in the sub-channels. This is called the Kelvin-Helmholtz instability.

The Kelvin-Helmholtz instability in a single phase flow occurs when there is a velocity difference between flow-lines. This velocity difference creates shear stresses that result in vortices being formed at the boundary of this instability. This principle takes place in turbulent and laminar flow regimes, and the resulting vortices are periodic in nature. The Kelvin-Helmholtz instability also occur in the rod bundle geometry. Flow velocities are different in the gap then in

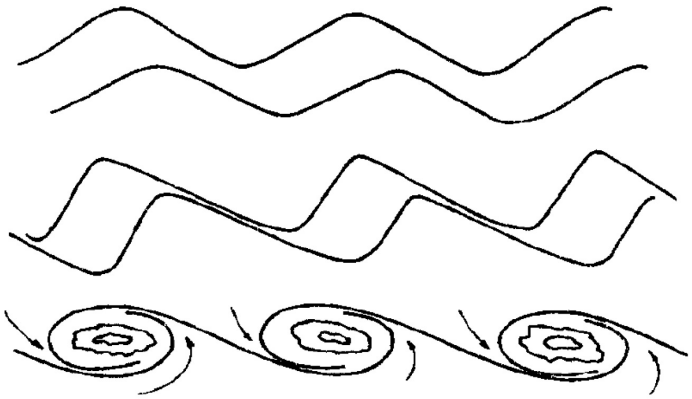

Figure 3.2: Creation of coherent structures as a result of the Kelvin-Helmholtz instability

the sub-channels resulting in shear stresses. These kind of velocity differences were explored by Mahmood (2011) for simpler geometries. To solve these stresses large vortices are created along the flow, see figure 3.2. A schematic pictures of the flow is presented in figure 3.3 to illustrate the formation of coherent vortices. The vortices created along the boundaries of the gaps and sub-channels are presented in figure 2.1. These vortices are the structures responsible for the cross-flow mixing between different sub-channels, and it is these specific structures that are being investigated with this research.

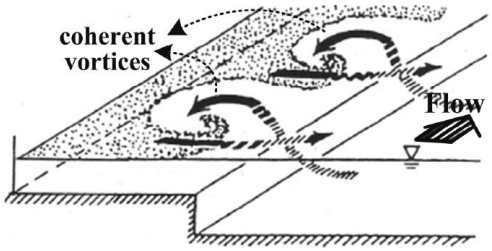

Figure 3.3: Structures occur due to the velocity difference between the two flow channels.

3.3 Objectives

The objectives of this research are as follows:

- To reproduce the preliminary results of Bulk in the rod-bundle geometry.
- To further develop the data analysis methods to reduce noise, and expand power spectral density analysis to produce better insight in flow characteristics.
- The last objective is to find the cross-flow vortices or structures for laminar, transitional and turbulent flow, and to quantify their size.

Chapter 4

Rod-Bundle Setup

The current research has been conducted on the set-up used by Bulk (2012). The experimental setup is based on the setup used for the LDA measurements of Mahmood. The set-up consists of a 6.64m long 'flow tower' as pictured in figure 4.1. This tower is made up of six 1-meter-long Polyvinyl Chloride (PVC) sections and one specially designed measurement section. Parts of solid PVC rods were placed on the sides of the sections, and four hollow rods where used to simulate a large rod-field. The four hollow PVC pipes held in place by metal spacers to ensure the desired geometry was continuous. Furthermore, the rods in the system are hollow and open at the top to ensure they are fully filled with water. This increases their weight and reduces the effect of normal forces on the rods, and thus the geometry.

The geometry consists of nine sub-channels and ten gaps as indicated in figure 4.2. The defining property of this geometry is the diameter to pitch ratio D/P of 0,7 . This ratio has been chosen to successfully compare this research with the results of Ikeno and Kajishima (2010), Bulk (2012), and Mahmood (2011). The rods in this set-up have a diameter of 25 mm and a spacing between them of 10.7 mm. With applied geometry and dimensions the hydraulic diameter was evaluated to be; $D_h = 40mm$.

The hollow rods contained in the center of the setup are kept in place with metal spacers. These spacers are sunk into the rods to diminish influences on the flow. The parts of the spacers exposed to the flow have a thickness of 2mm. During the LDA measurements with this geometry, Mahmood found no measurable effect of the spacers on the flow.

To operate this set-up, the system is slowly filled from the bottom up until the tower-overflow is reached. At that moment the pump is started and the flow loop is initiated. Notice that the flow through the system is not directly regulated by a pump. Gravity acts as the driving force for the flow. The flow through the system is regulated by three different rotameters at the bottom of the flow tower.

4.1 Measurement Section

The setup used as such is not perfect due to the spacers and usage of PVC which is a weak material and might be subject to small deformations. Due to the introduction of two wire-meshes in the flow-loop, a custom measurement section was built. The measurement section consists of a custom build 0.64 m long section with 2 wire-meshes spaced 35.2 mm apart. The rods are made of aluminum to ensure the durability of the geometry. The two wire-meshes are situated at the bottom of this section so the closest metal spacer is situated 12,5 D above the upper wire-mesh. This is done to rule out any effect the spacers might have on the flow. The

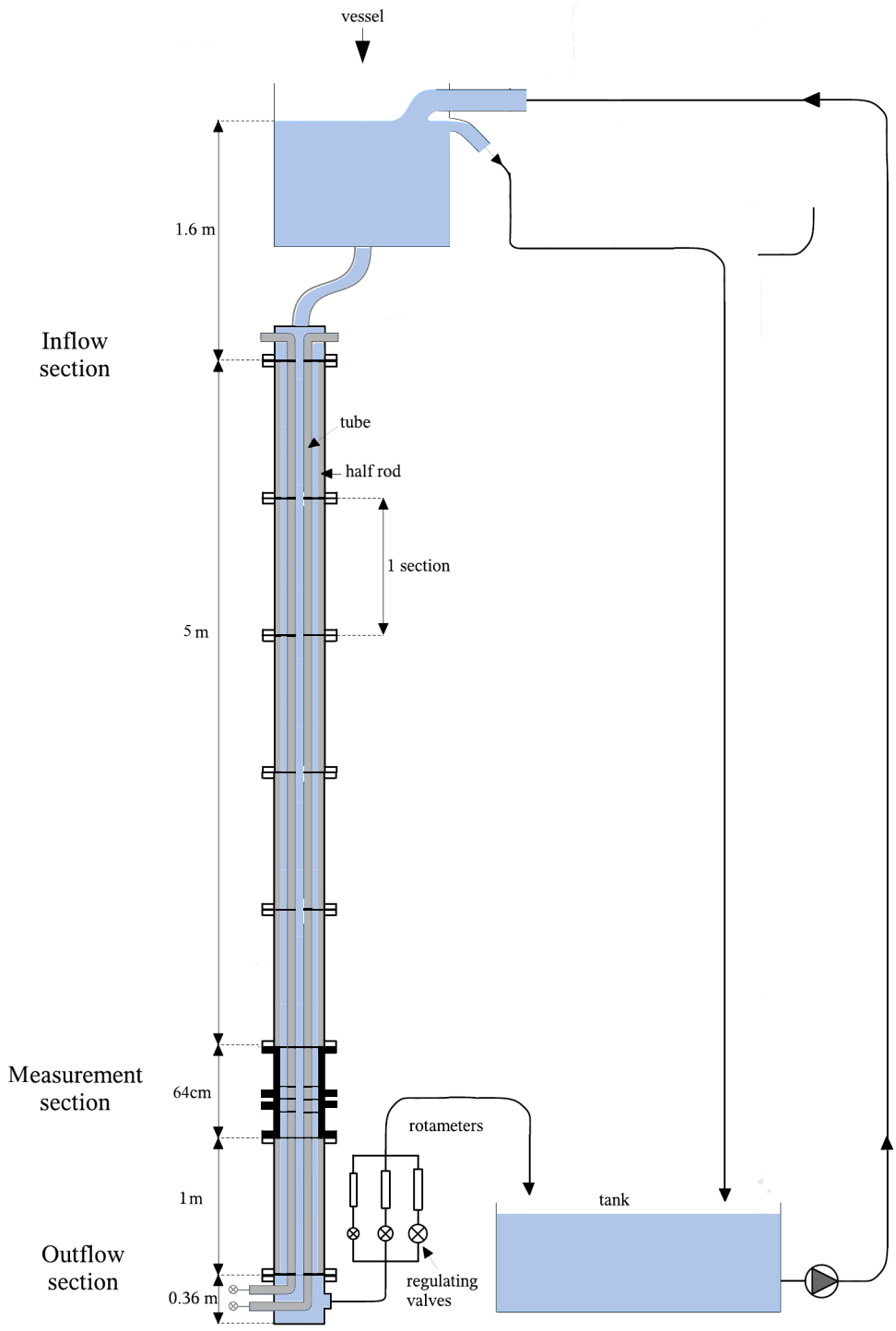

Figure 4.1: Schematic overview of the experimental set-up and its flowloop.

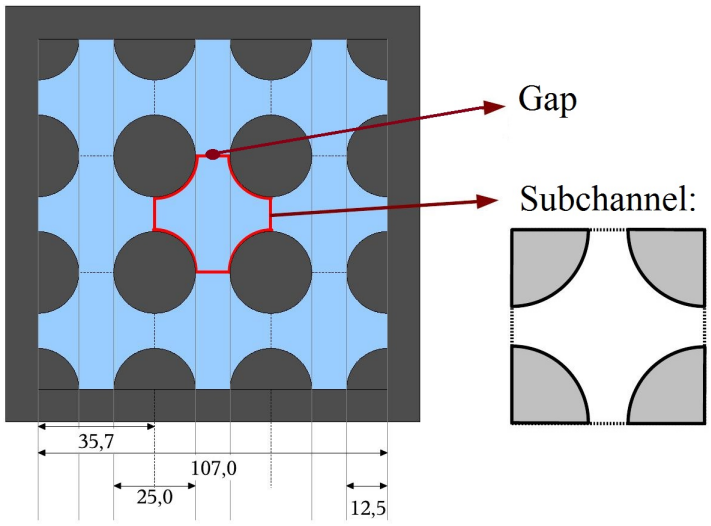

Figure 4.2: Diagram of the cross-section in the system.

measurement section is placed beneath five regular sections. This provides a length of 5.64 m for the flow to fully develop.

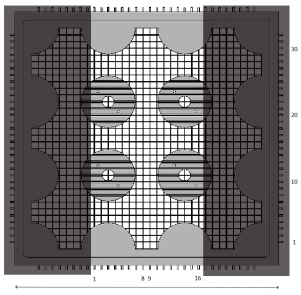

(a) The effective measurement surface of the wiremesh.

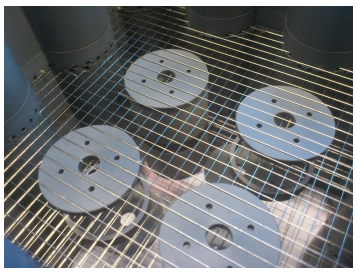

(b) Picture of the wire-mesh in the measurement section.

Figure 4.3: The installed wire-mesh in the rod-bundle setup. Figure 4.3a shows the effective measurement section of the wire-mesh. Figure 4.3b shows the installed wires in the setup.

4.2 Wire-Mesh

Measurement data was acquired by means of two wire-meshes. A wire-mesh, as presented by Prasser et al. (1998), consists of two perpendicular fields of wires spaced 3mm apart (transmitter wires and receiver wires) that are distanced 1.5 mm apart from each other and function as electrodes. The wire-mesh, together with the data acquisition box, is able to measure the conductivity at each crossing of wires. In this case the equipment measures the conductivity of the injected tracer (salt water) flowing with the water at each intersection of wires, thereby giving an accurate cross-sectional measurement tool. The conductivity is measured by transmitting a current through the transmitter wires and receiving the data through the receiver wires. The

data acquisition box only allows for 32 by 32 wires. To make sure that the area of interest of both wire-meshes was covered the transmitter wires were split across both wire-meshes, and only 16 receiver wires where used for each wire-mesh.

The limitations of the data acquisition box prevented the analysis of the complete cross-section. However, the area of interest for this particular study is fully covered by both wire-meshes. Figure 4.3a shows the effective measurement section of the wire-meshes and the main injection location. The two wire-meshes are separated by 35.2 mm and cover the same cross-sectional area, enabling the direct analysis of velocity through cross-correlation. This property will add data on the spatial measurement of structures. The covered intersections of wires are later referred to as pixels, where the precise location of a pixel can be seen in figure 4.3a.

Lastly, the distance between the wires of a single wire-mesh limits the measurement of very small structures. In general the eddies with size smaller then the distance between the meshes (1.5 mm) cannot be detected. The sensors, therefore, cannot measure all the way till the Kolmogorov scales.

4.3 Tracer Injection

To accurately measure the fluid flow with the use of a wire-mesh, a tracer with high conductivity compared to the flowing water must be used. Such tracer imitates the flow of thermal energy through a fluid and therefore gives insight on the heat dissipation and flow through the rod-bundle geometry. For this research a solution of salt was used as tracer. This tracer is cheap, easy to produce, and the results of Bulk with this tracer look promising. Following the recommendations of Bulk (2012) the tracer injection was done in the gap at $10D_h$ above the first wire-mesh, the highest available injection position. At this position the tracer dissipation yielded more promising results.

This setup has been used by Bulk. For further specifications his work provides full coverage of the setup.

Chapter 5

Results

The first part of this chapter will discuss the validation of results and the reproducability of Bulk's findings. Secondly the expansion of this research and its results will be presented.

5.1 Validation

The first goal of this research was to validate the retrieved data, and reproduce the results of Bulk (2012). Figure 5.1 shows a time frame of one measurement at Re 3000. The tracer was injected at a distace of 10 Dh above the top wire-mesh and in the gap. This figure shows that the tracer dispersion is relatively small and stays in the gap area. The general measured conductivity is of the same order of magnitude as the results of Bulk, and present the same dissipation at Re 3000. Furthermore, one can see that the lower wire-mesh measures a higher conductivity in the gap then the upper wire-mesh. This should not be the case due to the dispersion of the salt throughout the medium, one should expect the upper wire-mesh to measure higher concentrations of salt.

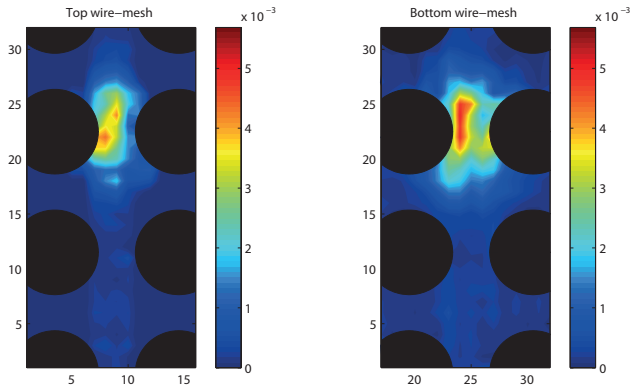

Figure 5.1: Slice of measurement at Re 3000

5.1.1 Cross-Sectional Mean

The tracer was injected in the gap between two rods. Analysis of the time average conductivity throughout the wire-mesh confirms that the tracer injection was done in the gap. Furthermore,

figure 5.2 shows that the dissipation of tracer is symmetric in each sub-channel. The mean values of concentration are consistent with the values found in the time frame of figure 5.1.

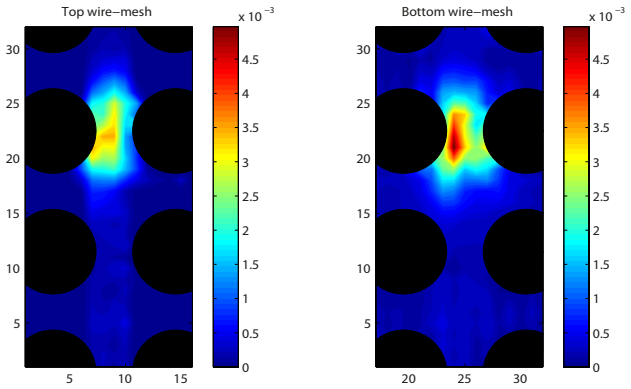

Figure 5.2: Mean conductivity of the tracer. The black areas indicate the rods.

The used wire-meshes show a slight difference in average output intensity. This bias between the two signals is probably the result of an intervention in the hardware. Early problems with the data acquisition box and system required the Wire-Mesh box to be repaired. The instalment of the repaired hardware during Bulk's study prevented a thorough new calibration of the wire-meshes. Due to the extent of this study no further steps were taken to recalibrate the wire-mesh box. Furthermore, the biased difference between the two wire-meshes was accepted, as it would not influence the periodicity of the relevant flow characteristics.

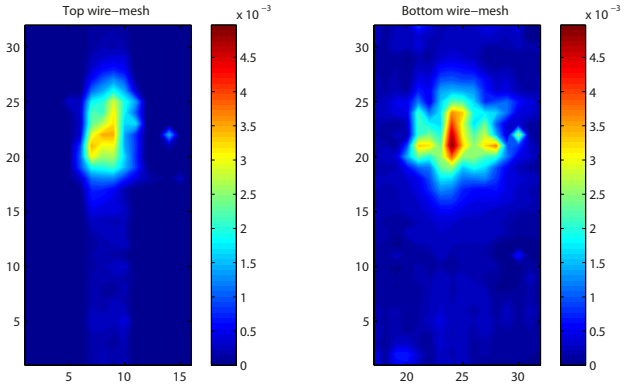

Figure 5.3: Mean conductivity of water with the black patches removed.

5.1.2 High signal in rods

During the course of this research unusually high levels of conductivity were measured in the rods as can be seen in figure 5.3. These high values of conductivity inside the rods did not appear to be constant for every measurement. This high signal does not have any influence on the periodicity of the flow, and as such does not disturb the measured flow characteristics. To

eliminate further 'influence', the second wire-mesh was used for all spectral analysis of relevant flow properties.

5.1.3 Time signal

The foremost use of wire-meshes before now was to measure flow development in multiphase flow, as it gives accurate spatial data set. Te flow of tracer as a function of time is shown in figure 5.4. The left figure shows the flow through the upper wire-mesh, while the right figure shows the flow through the lower wire-mesh.

Consistent with expectations, the flows show some correlation between the two wiremeshes with a timelag. This measurement is smoothened in the streamwise distance to reduce noise. Furthermore, the bias found in figure 5.1 and 5.2 can be seen here. The bias does not influence the time lag that maximizes the correlation, and therefore does not influence the determination of the concentration velocity.

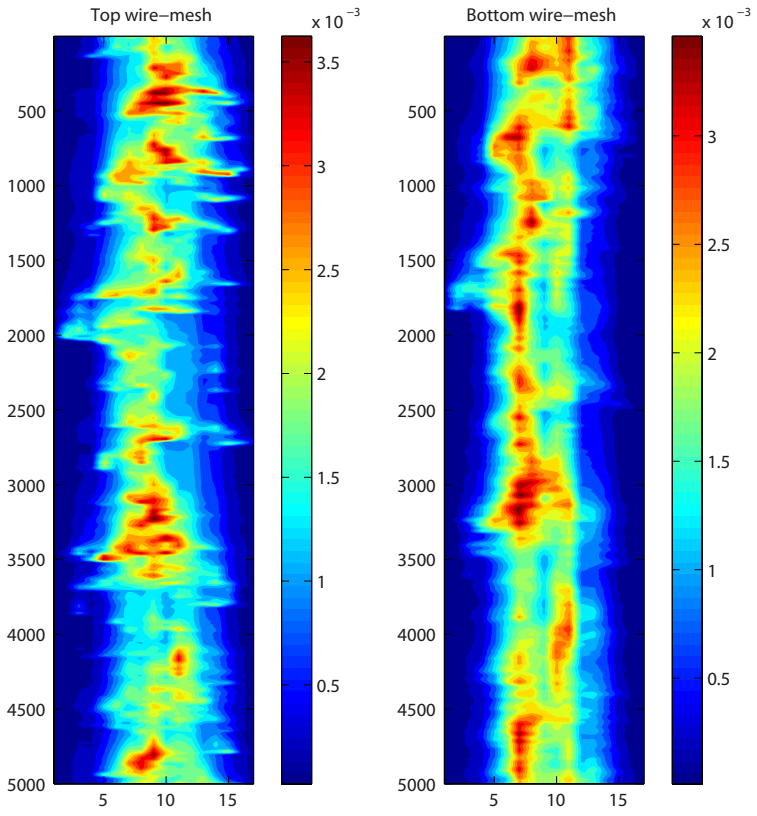

Figure 5.4: A slice in time of the tracer flow through the gap.

5.2 Cross-correlation & Velocity

The correlation detected in figure 5.4 can be quantified through the cross-correlation of both wire-meshes. By cross-correlating two data pixels at the same location on different wire-meshes,

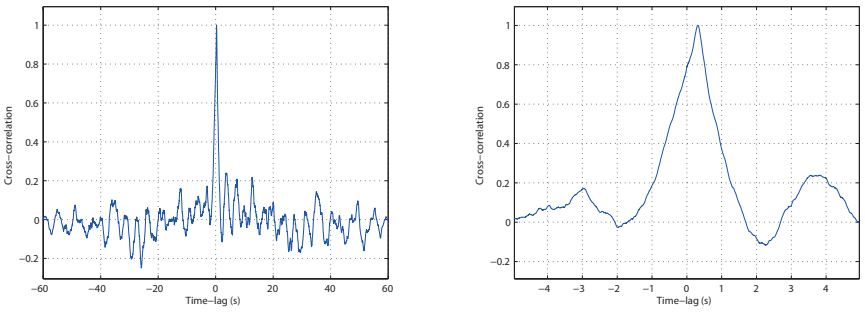

Figure 5.5: Cross-correlation of the the two wire-meshes at Reynolds 3000

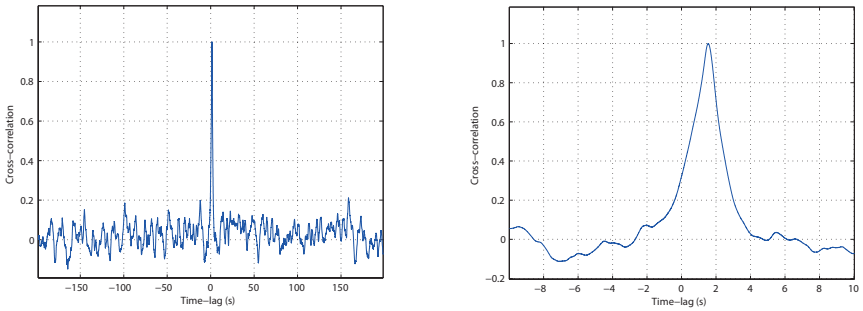

Figure 5.6: Cross-correlation of the the two wire-meshes at Reynolds 500

one can find the time lag that maximizes the correlation. Figures 5.5 and 5.6 show the cross-correlations of measurements at Re 3000 and Re 500. These correlations show a clear peak near t = 0. After zooming in the time lag becomes more visible. The time-lag at Re 500 is about 6 times larger then at Re 3000, which is consistent with the linear behaviour of Reynolds numbers with respect to velocity. Knowing the time lag and the distance Δh between the two wire-meshes, the tracer velocity can be determined using the simple formula:

$$v_{tracer} = \frac{\Delta h}{timelag} \tag{5.1}$$

This yields a tracer velocity of 1.2 for Re 3000 and 0.2 for Re 500 for the given cross-correlations of figures 5.5 and 5.6. This is slightly above the calculated bulk velocities of $0.084 m/s$ and $0.014 m/s$.

This technique can be expanded to determine the velocities of the measurement points, thereby obtaining the velocities of the complete cross-section. To reduce the uncertainty, the velocity of all measurements at the same Reynolds number were added together to obtain the mean cross-sectional velocities at the given Reynolds numbers. This has been done for a range of Reynolds numbers. Average flow velocities of all measurements at Re 6000, 3000, 1000 and 500 are presented in figure 5.7. The dark red areas define the area where no tracer was measured, and therefore the velocity could not be determined. All measurements have been normalized by

the calculated bulk velocity, v_{bulk}.
The overall velocities are higher than the calculated bulk velocity. For the measurements at different Reynolds numbers, the average tracer velocity in the gaps is approximately 25% higher than the measured velocity in the channels.

The average velocities of the tracer in the channel (pixel 17:8) and gaps (pixel 22:8) have been plotted in figure 5.8 as a function of Reynolds number. The overall character of these velocities as a function of Reynolds is linear, as expected, and the values are in the same order of magnitude as v_{bulk}. The gap velocity, however, is significantly higher than the channel velocity for all Reynolds numbers.

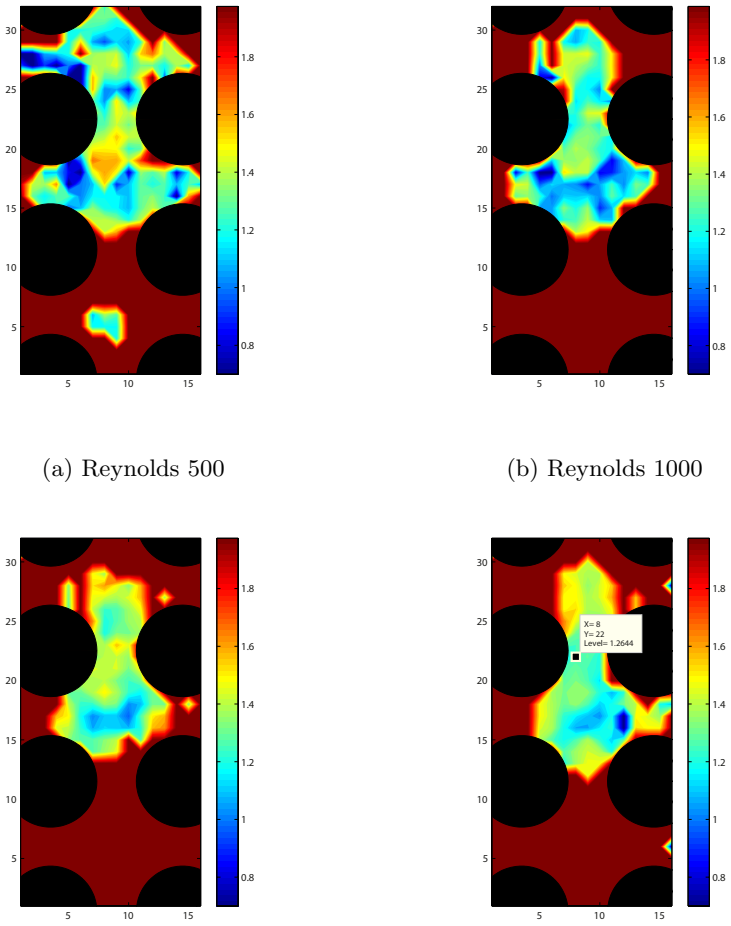

(a) Reynolds 500

(b) Reynolds 1000

(c) Reynolds 3000

(d) Reynolds 6000

Figure 5.7: Mean Velocity Cross-Sections at indicated Reynolds numbers. The dark red areas indicate the area where no tracer was measured.

Using the LDA setup, Mahmood measured the velocity profiles in different geometries. His results are presented in figure 5.9, and show the velocity profiles at flows of Reynolds 3153 and

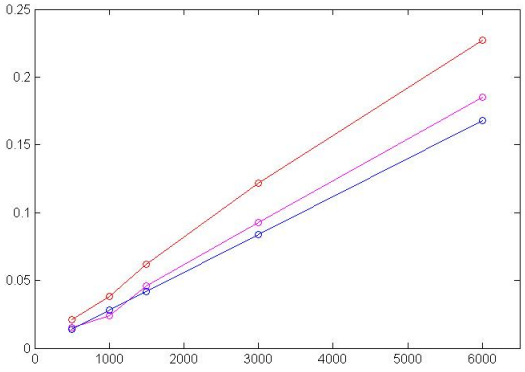

Figure 5.8: A plot of the found velocities as a function of the Reynolds numbers.

631 normalized by the bulk velocity. The minima of the left graphs should be the same as the maxima of the right graphs. From his findings we can deduce that the average velocity in the center of the gaps and sub-channels is higher then the bulk velocity. The results of figure 5.7 show that the measured velocities are of the same order of magnitude as Mahmood. However, the results are in contrast with the profile presented in figure 5.9 where the velocities of the gaps are lower then the velocities in the sub-channels. This strong difference in velocity profile is peculiar. This difference might arise due to the fact that two different measurement techniques are used.

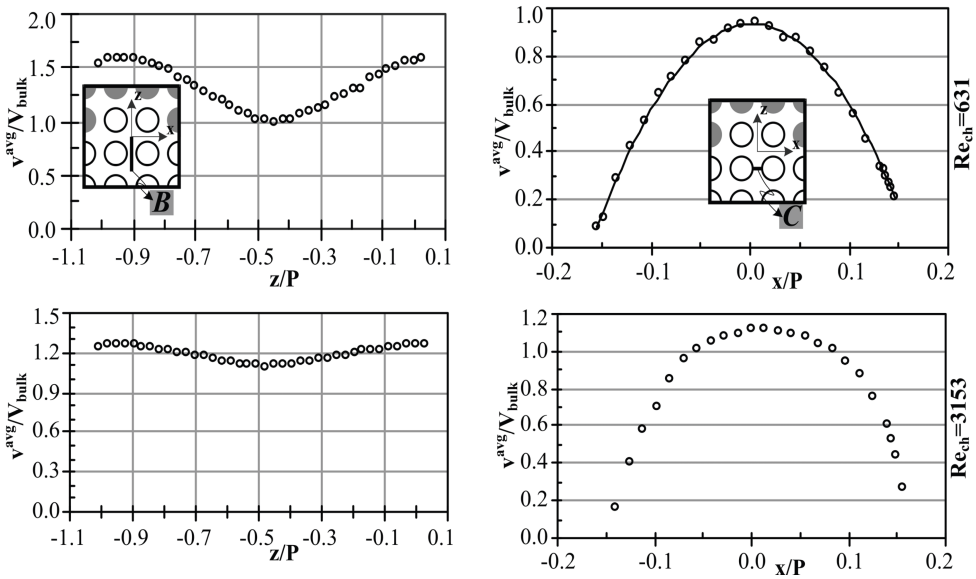

Figure 5.9: Streamwise velocity measurements by Mahmood (2011).

5.3 Structures

This section presents the main results of this research. Firstly, the analysis of the autocorrelation of time signals of single measurement points is presented. This is further investigated with power spectral density analysis in the second part, while the third part offers the results on structure length and width.

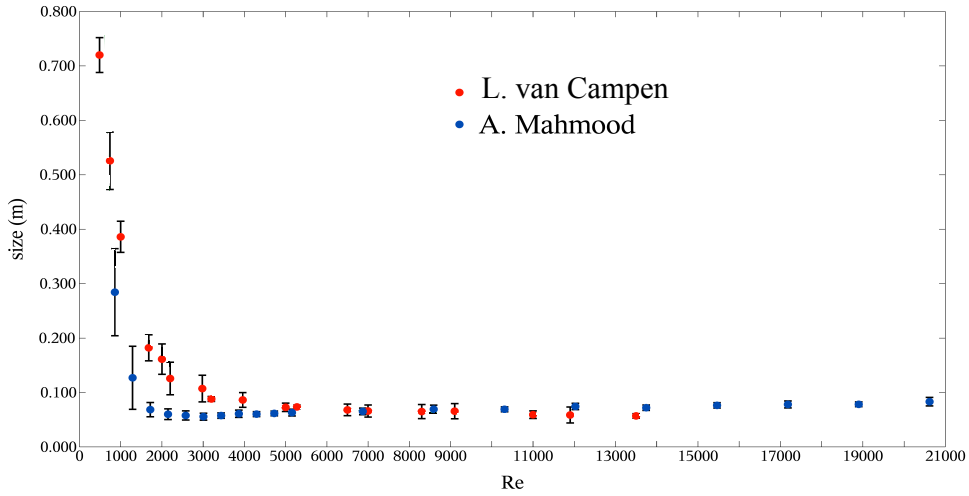

Figure 5.10: Structure streamwise-size in the rod-bundle geometry as a function of the bulk Reynolds number, found by Mahmood (2011) and van Campen (2009) using LDA measurements.

Having acquired localized velocity data of the injected tracer through the cross-correlation of time signals, it is now possible to transform the measured data as a function of streamwise length. To look for the coherent structures presumed to be present, autocorrelating the data of one pixel yields clear results. Measurements were performed at flows ranging from Re 500 to Re 6000. Figure 5.11 shows the normalized autocorrelation of pixel 21:9 for flow at Re 6000 and Re 500 as a function of distance. The turbulent flow at Re 6000 shows a clear periodicity in the autocorrelation. Each peak represents a structure passing through the wire-mesh. Furthermore, the periodicity dies out as the distance with the first structure becomes very large. The presented autocorrelation of Re 6000 indicates a structure length of 0.25 m.

The flow at Re 500 does not yield such clear periodicity. The autocorrelation shows a peak of 1 at 0 which than drops sharply to 0. After that practically no correlation can be seen, which follows the autocorrelation pattern of noise. Furthermore the expected increase of structure size is not visible. One possibility for this absence of large structures in the measurement data could be the physical limitations of the setup. As the pump has a small reservoir of 60 mL of tracer, and there is a limit in the amount of data possible to collect with the data acquisition box, it was not possible to measure for very long times. Because of this, the larger the structures become, the fewer are measured and this might therefore not yield sufficient statistical data. As all the measurements at low Reynolds numbers showed such behaviour we may carefully conclude that at these conditions only noise is measured.

Autocorrelation of flow at Reynolds 3000 was also performed. At this flow rate measurements yielded relatively good periodicity. However, the structure size determined by the autocorrelations varied a lot. Figure 5.12 shows the autocorrelation of flow at Reynolds 3000 for two mea-

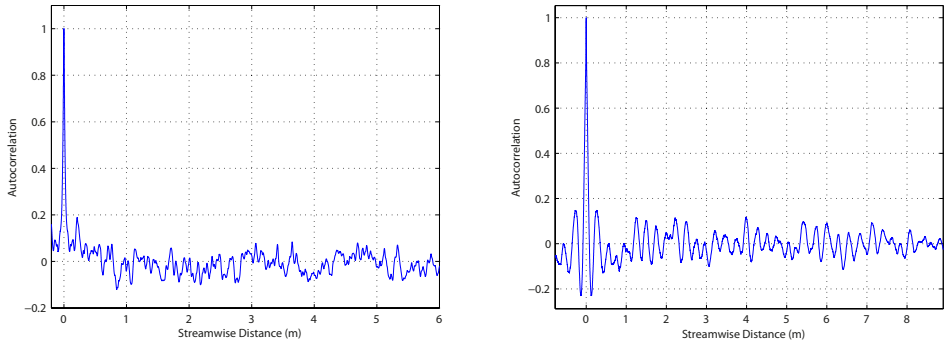

(a) Re 500 (b) Re 6000

Figure 5.11: Autocorrelation of pixel 21:9 at Reynolds 500 and Reynolds 6000.

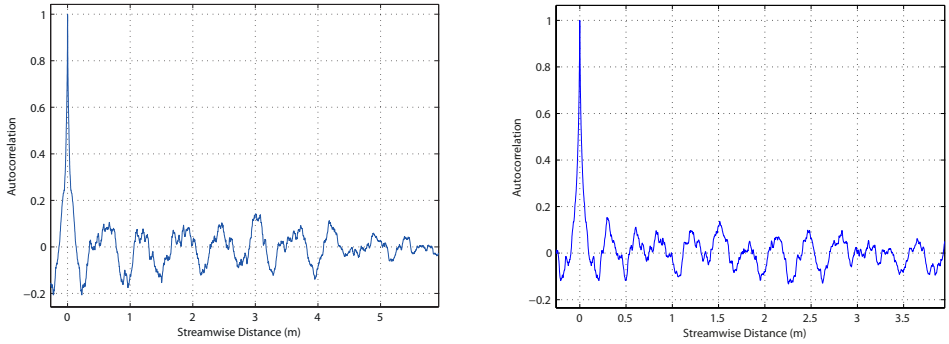

Figure 5.12: Autocorrelation of pixel 21:9 at Reynolds 3000. There is a clear difference in correlation frequency between the two measurements.

surements taken at different moments. The measurement on the left indicates a structure size of 0.7 m (double that found by Bulk), while the measurement on the right indicates a size of 0.34 m. Such variations were found for multiple measurements, which suggests that the structures are not precise and well defined for a given flow.

The results found for the autocorrelation of the time signals seem to be in general accordance with Bulk for high Reynolds numbers. However, lower Reynolds numbers did not yield the expected results. Furthermore, the results compared with the findings of Mahmood and van Campen in figure 5.10 suggest that the structure sizes may be larger than initially presumed. Localized velocities through the cross-correlation give a more reliable result then Mahmood and van Campen as they made some significant assumptions on the flow velocities due to the limitations of the LDA setup.

5.3.1 Power Spectral Density

The autocorrelation of the time signals of individual pixels was performed to obtain relevant results on the characteristics of the cross-flow structures. Autocorrelating the time signal directly

filters out noise. Single measurements proved to be very noisy and unreliable. The preliminary results of Bulk at short time measurements were unreproducible for longer measurements showing great deterioration of periodicity. To obtain full understanding of the measured flow in the rod-bundle geometry and its comprised flow frequencies, power spectral density analysis was performed on the autocorrelation of the time signals of individual pixels on the wire-mesh. Power spectral analysis gives insight in the flow frequencies of he measurements. It is a powerful tool to quantify structures in flow. Power spectral analysis of autocorrelations of single measurements proved to be very noisy. To remove part of this noise, the PSD spectra of all measurements at the same pixels were added together. This has great effect on the time signal analysis, but due to the superposition principle of the frequency domain it greatly reduces the noise of power spectral density analysis. Figure 5.13 shows the power density spectrum at Reynolds 3000 of combined time signals through pixel 20:9. Though the figure still shows significant noise, three regions can be distinguished. Starting from the left there is a region where the signal is nearly horizontal, showing that these frequencies are equally present in the flow. After that a region of linear decay can be found followed by a region with steeper decay. After a frequency of 60Hz no signal can be measured. Though this power spectrum shows different regions, no clear peak can be found.

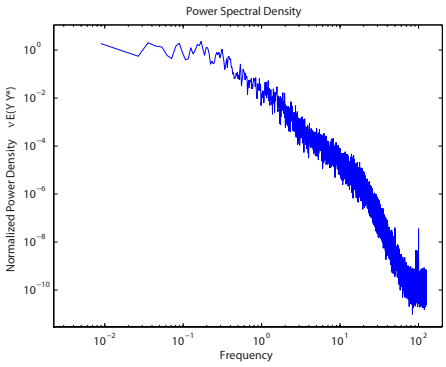

Figure 5.13: Power spectral density of combined time-signals of different measurements at Reynolds 3000

5.3.2 Pre-Multiplied Power Spectra

To get a better view of the relevant flow frequencies and their energies, pre-multiplied power spectra yield were created. Pre-Multiplied Power Spectra(PMP Spectra) filter out irrelevant frequencies and give a clearer view of the measured flow frequencies that contain most of the flow energy. This is done by multiplying the power spectrum with the corresponding wavenumbers.

$$\Phi = E \cdot \nu \tag{5.2}$$

Where the wavenumber is specified by

$$\nu = \frac{f}{\langle U \rangle} = \frac{1}{\lambda} \tag{5.3}$$

Analysis of these PMP Spectra give important insight on the frequencies present in the flow and their energies. The PMP Spectra are plotted as a function of the inverse of the wavenumbers

corresponding to the frequencies, and are a direct measure of the longitudinal lengths of eddies or structures at that frequency.

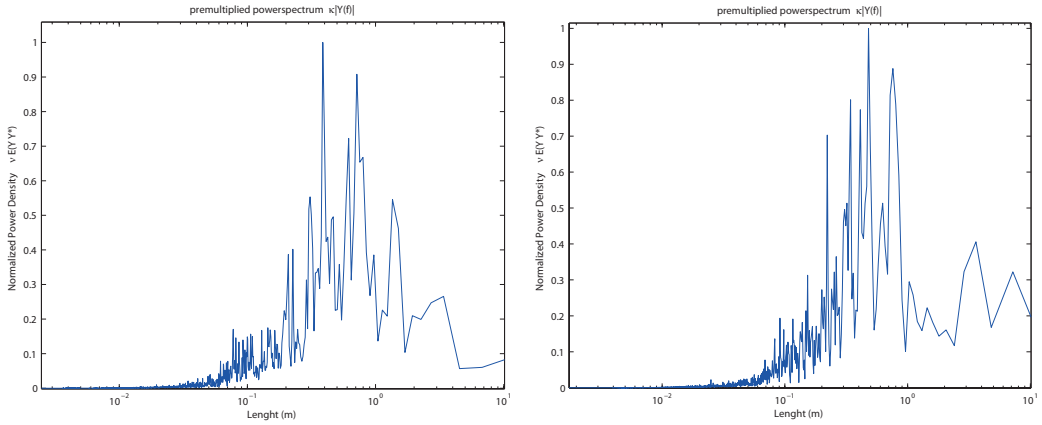

(a) Pixels 20:24 and 20:25

(b) Pixels 19:24 and 19:25

Figure 5.14: Pre-Multiplied Power Spectral Density plots of the combined measurements of geometrical pixels

The spectra were further enhanced by adding pixels in symmetrical positions in the geometry together. Figure 5.14 shows the combined PMP Spectra at Re 3000. As the PMP spectra are of the same form and order of magnitude, this analysis was extended to the whole gap area, adding all measurement data of the gap region together to eliminate noise. The results are presented in figure 5.15 for the power spectra, and in figure 5.16 for the PMP spectra. The power spectra of figure 5.15 show a great decrease in noise. Furthermore, the spectra of flow at Reynolds 6000 shows a clear peak which identifies a dominant frequency and thus a dominant structure size. This is more easily noticable in figure 5.16.

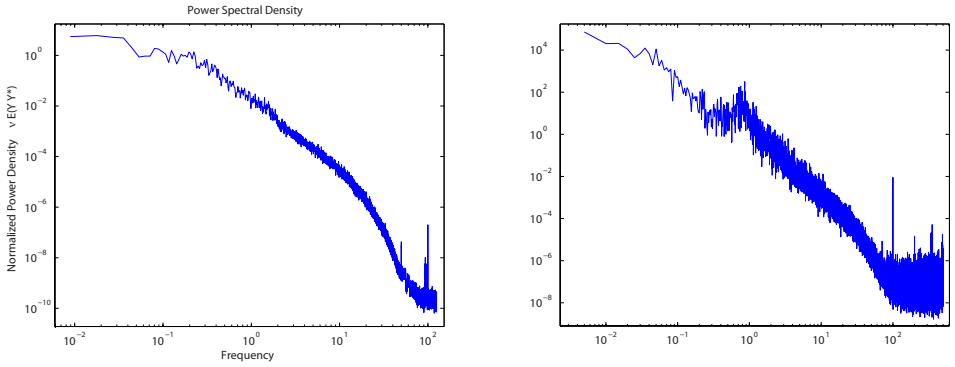

(a) Reynolds 3000

(b) Reynolds 6000

Figure 5.15: Power Spectrum at Reynolds 3000. This is a combined spectrum of all data points across the gap region, thereby diminishing the noise.

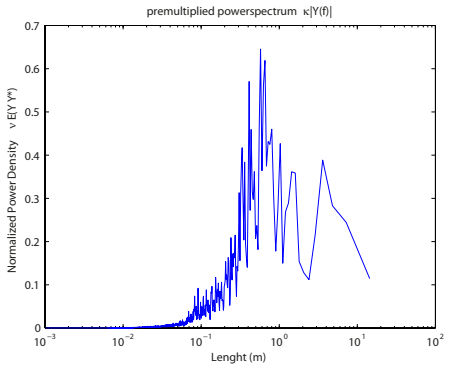

(a) PMP spectrum at Reynolds 3000

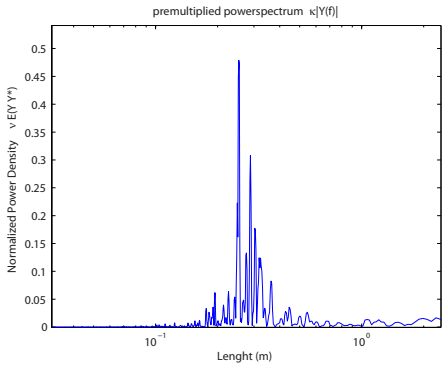

(b) PMP spectrum at Reynolds 6000.

Figure 5.16: PMP Spectra created with the combined measurement data of the whole gap-region

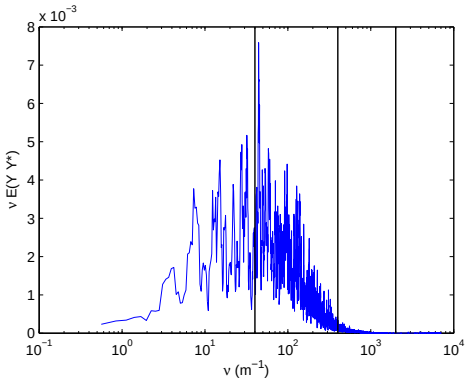

(a) PMP spectrum of pipeflow at Reynolds 17800 as measured by Bulk (2012)

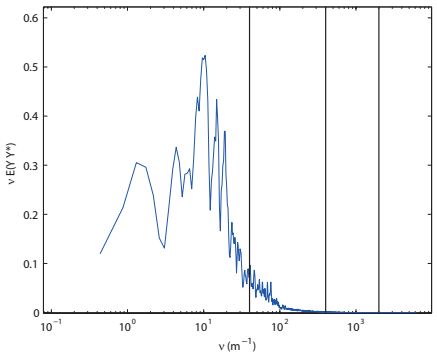

(b) PMP spectrum at Reynolds 3000 as a function of wavenumber..

Figure 5.17: PMP Spectra created with the combined measurement data of the whole gap-region

Bulk (2012) did research on pipeflow using a wire-mesh and produced some PMP spectra. Though his spectra were made for measurements in a different geometry and at a different Reynolds number, it does serve as a comparison with fully turbulent flow without structures. Figure 5.16a compares the results of Bulk with the result of figure 5.16a as a function of wavenumber. The vertical lines help to distinguis three regimes in the pipeflow measurements of Bulk. These lines have also been plotted in figure 5.16b to help compare the two figures. It is clear that the bulk of the flow frequencies in a rod-bundle geometry lies in the low wavenumber region. Regular turbulent flow has eddies of the same order of magnitude as the hydraulic diameter. However, this study shows that the longitudinal lengths of structures at Reynolds 3000 is much larger then at regular turbulent flow. We may therefore conclude that large structures are present in a rod-bundle geometry. These results are still noisy, but show an average structure length of 10 D_h to 25 D_h.

5.3.3 Correlation Width

A study was performed to obtain the average width of correlation in the flow section. This analysis was performed for all measurements at Reynolds 3000. Figure 5.18 shows the average correlation of a single pixel on the second wire-mesh with all the other pixels on the same wire-mesh. The correlation over the cross-section shows a correlation width of 4 to 5 pixels corresponding to 20 mm or $0,5D_h$, which is an indication of the structure width at Reynolds 3000. Furthermore, the found structure width is symmetric around the gap, which corresponds to the expectations that the structures alternate between two adjacent sub-channels.

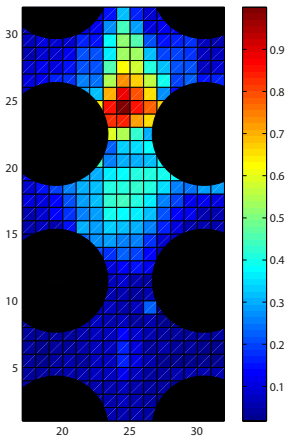

(a) Pixel 24:24

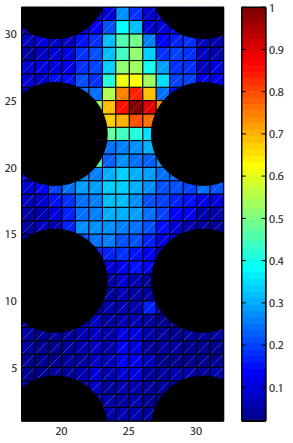

(b) Pixel 24:25

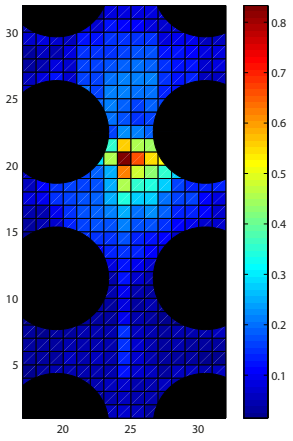

(c) Pixel 20:24

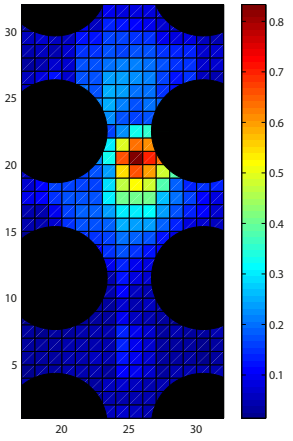

(d) Pixel 20:25

Figure 5.18: Correlation of pixels width the rest of the wire-mesh indicating the width of structures

Chapter 6

Conclusions

6.1 High Conductivity in Rods

The origin of the high transmittance in the rods could not conclusively be indentified. The system has been thoroughly flushed with clean water, as well as the interior of the pipes. No change was seen as a result of these measures. This signal inside the rods seems to be increasing, and might be an indicator of some wearing or erosion on the wires.

6.2 Velocity

The velocity of the injected tracer has been calculated for different Reynolds numbers across the cross section of the wire-mesh. The velocity of the tracer is larger then the calculated bulk velocity, by an average factor of 20% in the gap. The overall velocity across the cross-section is higher than the bulk velocity. This is probably due to the varying hydraulic diameter of the different channels. The hydraulic diameter of the outer channels is smaller due to the outer PVC wall, which may result in slower velocities in the outer channels. Furthermore, the conclusions of R. Bulk presenting an homogeneous velocity across the cross-section can be rejected. This research shows an inhomogeneous velocity with maxima at the gaps where the structural vortices are expected to be found, and clear minima in the channels.

6.3 Structures

Initial analysis of flow in the rod-bundle geometry proved to be unsuccessful. The results of Bulk (2012) were reproduced, but could not be expanded to longer measurements. Furthermore, analysis of single measurements showed measurements where not repeatable under matching circumstances and conditions. The thus obtained results were inconsistent and unreliable. We may conclude that the preliminary results obtained by Bulk, though they proved the system works, are unreliable.

With the obtained data a second analysis method was used, in which the measurements of identical frequencies were added together. This method was mainly performed at Reynolds 3000 and yielded more complete results. As viewed in the previous chapter, the obtained power spectral densities define a band of frequencies present in the flow, that are in contradiction with the frequencies found in literature for regular turbulent flow in a pipe or geometry with a characteristic diameter of 4 cm. The results produced with the second analysis method may

indicate that the structural flow in a rod-bundle geometry is not as well defined as expected. The composition of these structures should be further investigated for different Reynolds numbers.

The pre-multiplied power spectra give an indication of the length of the structures at Reynolds 3000. Structures with lengths ranging from $10D_h$ to $25D_h$ are present in rod-bundle flow at Reynolds 3000. Analysis of the correlation of pixels with the rest of the field give an indication of the width of the structures. Preliminary conclusions can be made on the width of these structures. Structures have an average width of 4 pixels which corresponds to $0.5D_h$ The correlation was found to be symmetric for either side of the channel.

These scales show that structural flow in a rod-bundle geometry with characteristic diameter of 4cm is not as regular and homogeneous as expected. The aspired structures might be irregular and could be bulk structures build up of smaller more turbulent-like structures.

The same analysis was performed for lower reynolds numbers, 500 - 1500. The results showed clear electrical noises at 50Hz and some flow noises. We may carefully conclude that no structures were present at these flow rates.

Chapter 7

Recommendations

For continued research on structural flow in a rod-bundle geometry the following recommendations can be made.

- The high conductivity measured in the rods could present more complicated problems in the future. The wire-mesh should therefore be checked for wear or corrosion inside the rods.
- To produce reliable measurements at lower Reynolds numbers, the set-up should be improved in the following ways. More accurate flow regulators for very low Reynolds numbers should be installed, as oscillatory behaviour can be observed in the smallest regulator at flows lower then 1000 Reynolds. The injection mechanism should be improved to allow for a bigger injection reservoir or for longer injection of the tracer. A continuous pump with a big reservoir operating at the desired regime or a combination of several regular pumps combined can be considered, though not available at the moment.
- A recalibration of the wire-mesh should be performed to correct the current bias between the upper and lower wire-mesh.
- Consistent and accurate measurements of flow in the turbulent regime should be made in order to confirm the literature. The used analysis method should be further tested at turbulent and more operational flow rates.
- Analysis has been performed to determine the phase lag that maximizes the cross-correlation between structures flowing through the same gap but in two different adjacent channels. This analysis has, however, not yielded any sensible results due to the lack of salt and slow dispersion in the cross-sectional direction. To further analyse this phase lag, one should consider inserting the tracer at a higher injection point. Another, and probably more accurate, method would be to inject the same tracer in two adjacent channels. Structures should clearly create a time lag in the cross-correlation of these two channels.

Bibliography

R. Bulk. An experimental study on cross-flow mixing in a rod-bundle geometry using a wire-mesh. Master's thesis, Delft University of Technology, 2012.

T. Ikeno and T. Kajishima. Analysis of dynamical flow structure in a square arrayed rod bundle. *Nuclear Engineering and Design*, 240:305 – 312, 2010.

Pijush K. Kundu and Ira M. Cohen. *Fluid Mechanics*. Elsevier Academic Press, 3 edition, 2000.

A. Mahmood. *Single-Phase Crossflow Mixing in a Vertical Tube Bundle Geometry*. PhD thesis, Delft University of Technology, 2011.

H.-M. Prasser, A. Böttger, and J. Zschau. A new electrode-mesh tomograph for gas-liquid flows. *Flow Measurement and Instrumentation*, 9:111–119, 1998.

D.S. Rowe, B.M. Johnson, and J.G. Knudsen. Implications concerning rod bundle crossflow mixing based on measurements of turbulent flow structure. *Internation Journal of Heat and Mass Transfer*, 17:407 – 419, 1974.

L.J.A.M. van Campen. An experimental investigation on the use of fep as refractive index matching material for lda in a rod bundle flow. Master's thesis, Delft University of Technology, Delft, 2009.

A. Ylönen, W.-M. Bissels, and H.-M. Prasser. Single-phase cross-mixing measurements in a 4 x 4 rod bundle. *Nuclear Engineering and Design*, 241:2484 – 2493, 2011.